Bull Volcanol (2006) 68: 377–393
DOI 10.1007/s00445-005-0020-y

RESEARCH ARTICLE

Rikke Pedersen · Freysteinn Sigmundsson

Temporal development of the 1999 intrusive episode in the Eyjafjallajökull volcano, Iceland, derived from InSAR images

Received: 10 November 2004 / Accepted: 29 August 2005 / Published online: 7 December 2005

Abstract Eyjafjallajökull volcano, located in southern Iceland, is characterized by its quiet nature. Only about a handful of earthquakes associated with the volcanic system had been detected prior to the 1990s. Earthquake swarms did, however, occur in 1994 and 1999. Here we investigate the spatio-temporal evolution of a magmatic intrusion associated with the 1999 earthquake swarm via analysis of produced surface deformation. A series of interferometric synthetic aperture radar (InSAR) images, spanning various periods of the intrusion, show that in 1999 surface deformation occurred mainly on the southern flanks of the volcano. The deformation amounts to more than 20 cm of range change. Inverse modeling resolves the deformation source to be a sill intrusion at 6.3 km depth. Sill opening was up to 1 m and the total intruded volume amounts to ~0.03 km^3. The InSAR data display a migration of the center of deformation through time, enabling us to create time-dependant sill-opening models. Furthermore, we investigate the spatio-temporal distribution of earthquakes and find that the distribution supports the InSAR derived model and additionally provides indications for a possible site of a feeder channel. Magmatic flow-rate estimates indicate an initial intrusion rate of 4–6 m^3/s, declining over a few weeks.

Keywords Iceland · volcano · Intrusion · Sill · Seismic swarm · Deformation · InSAR

Introduction

Temporal and spatial visualization of magma transport and emplacement beneath volcanic structures is an important element in the attempt to obtain a comprehensive understanding of volcanic processes. Improved knowledge of volcanic processes working at depth may advance capabilities for making competent forecasting of future volcanic eruptions. Recent advances in geodetic techniques such as continuous GPS and interferometric synthetic aperture radar images (InSAR) enable, throughout the volcanic eruption cycle (Dzurisin 2003), spatial and temporal visualization of surface deformation caused by magmatic processes at depth. Studies of magmatic intrusions have the potential of revealing some of their physical aspects, e.g., magma-migration paths, flow rates and stress conditions. Inverse modeling of surface deformation measurements may provide information about magma transfer and the shape, size and evolution of sub-surface magma bodies, given a set of prior assumptions. In this paper, we investigate the spatio-temporal development of an intrusion in the Eyjafjallajökull volcano, South Iceland that occurred in 1999. Our extensive InSAR dataset provides an opportunity to analyze and model the surface deformation field produced by a single intrusion event, spanning several months, into a significant volcanic structure exhibiting infrequent magmatic activity.

Editorial responsibility: H. Shinohara

R. Pedersen (✉) · F. Sigmundsson
Nordic Volcanological Center, Institute of Earth Sciences,
University of Iceland, Askja, Sturlugata 7,
101 Reykjavík, Iceland
e-mail: Rikke@hi.is
Tel.: +354-525-5483
Fax: +354-562-9767

Eyjafjallajökull volcano

In Iceland, the mid-Atlantic plate boundary is expressed as a series of seismic and volcanic zones (Fig. 1a). In southern Iceland the ridge is divided in two spreading segments, the Western and Eastern Volcanic zones (WVZ and EVZ respectively), with the EVZ being the current main locus of spreading. The South Iceland Seismic Zone (SISZ) is a transform zone connecting the two spreading segments. Eyjafjallajökull volcano is situated south of the intersection between the SISZ and the EVZ. The area is characterized by significant topographic relief and a lower spreading rate than the EVZ. In contradiction to tholeiitic products in the axial rift zone further north, volcanic products here belong to the alkaline or transitional suite, and the area is, based on the petrological difference as well as poorly developed extensional fractures, characterized as a

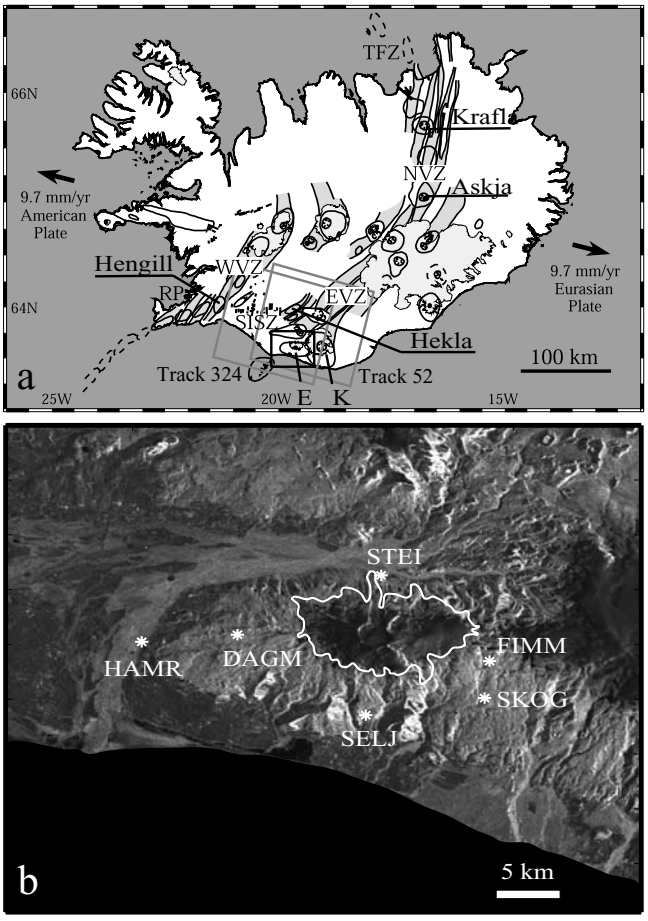

Fig. 1 **a** Volcanic systems of Iceland with their fissure swarms, central volcanoes and calderas—according to Einarsson and Sæmundsson (1987). Icecaps are also *outlined*. The plate boundary is divided into the Tjörnes Fracture Zone (TFZ), the Northern Volcanic Zone (NVZ), the Eastern Volcanic Zone (EVZ), the Reykjanes Peninsula (RP), the Western Volcanic Zone (WVZ) and the South Iceland Seismic Zone (SISZ). *Large boxes* delimit the ERS frames used. *K* Katla Volcano; *E* Eyjafjallajökull. The *rectangular box* delineates the area shown in Figs. 1b, 2a, 2b, 3, 4 and 8 (−19.2 to −20.2 °E, 63.8 to 63.4 °N). **b** SAR amplitude image of the Eyjafjallajökull area. The *white line* outlines the Eyjafjallajökull glacier. Locations of GPS stations in the area are shown with white stars

volcanic flank zone (Sæmundsson 1979). Eyjafjallajökull is an icecap covered stratovolcano rising to an elevation of 1,666 m.a.s.l. (Fig. 1b). The icecap covers an area in the summit region of about 80 km^2 in size, making interferometric measurements unattainable within this area throughout the year.

Volcanic activity in the system is episodic, with only four eruptions in the last 1,400 years (Gudmundsson et al. 2005). Three events were associated with eruptions occurring in the neighboring volcanic system (Katla), which has led to theories of a mechanical coupling between the Katla and Eyjafjallajökull magmatic systems (Einarsson and Brandsdóttir 2000). However, the two neighboring volcanic systems show a remarkable difference in activity level, which may be taken as intrinsic evidence of their difference in temperature structure. The Katla system is one of the most active in Iceland. It is a hot system with a residing crustal magma chamber and eruptions that typically occur twice a century. It has had persistently high seismic activity for more than four decades, with most earthquakes being low-frequency events (Einarsson and Brandsdóttir 2000). The Eyjafjallajökull volcanic system appears to be a cold structure as it exhibits sparse, episodic, high-frequency earthquakes with few eruptions. In the period from 1979–1985, only three well-located earthquakes were detected as originating at the Eyjafjallajökull volcano (Einarsson and Brandsdóttir 2000). This level of activity was typical for the initial period of instrumental coverage between 1971–1991. The South Iceland Lowland (SIL) system operated by the Icelandic Meteorological Office uses three-component digital seismic stations (Stefánsson et al. 1993; Bövarsson et al. 1999; Jakobsdóttir et al. 2002). Eight stations are located within a distance of 100 km from the volcano, with the closest station at a distance of about 15 km.

The 1994 intrusive episode

After a long quiet period at Eyjafjallajökull, local seismographs began detecting earthquakes there in 1991. Micro-earthquake activity was detected throughout 1991–1994, and in late May, 1994, an earthquake swarm commenced. The largest earthquake had a magnitude of M_L=2.3, and of the 130 recorded swarm events, 86 were of local magnitude 1.2 and larger. Earthquake locations for events occurring throughout 1994 are shown in Fig. 2a. The total seismic moment of the 1991–1994 activity was about 6×10^{12} nm, half of which was released before measurable crustal deformation occurred in 1994 (Sturkell et al. 2003). Locations from the SIL database (2004) show that the earthquakes were basically confined to a cluster at the northern flank of Eyjafjallajökull, with depths ranging from 1 to 13 km. Approximately 50% were found between 4 and 6 km depth. Dahm and Brandsdóttir (1997) conducted a moment tensor study including data from a temporary locally deployed seismic network and interpreted the 1994 earthquake swarm as being due to intrusion of an E–W striking dike into the northern flank of the volcano. However, a crustal deformation study based on dry-tilt and limited GPS measurements (Sturkell et al. 2003) contrasts the dike model. Sturkell et al. (2003) interpreted the surface deformation as being caused by an inflating Mogi point source situated beneath the southern slopes of Eyjafjallajökull. A sill model providing a link between the spatially offset areas of main ground deformation and main earthquake activity was provided by an InSAR study (Pedersen and Sigmundsson, 2004). The InSAR data spanned the entire 1994 unrest episode, hence did not provide any temporal development of the intrusion to be accessed.

Renewed activity in 1999

In early July of 1999, another earthquake swarm commenced within the Eyjafjallajökull volcano. The largest

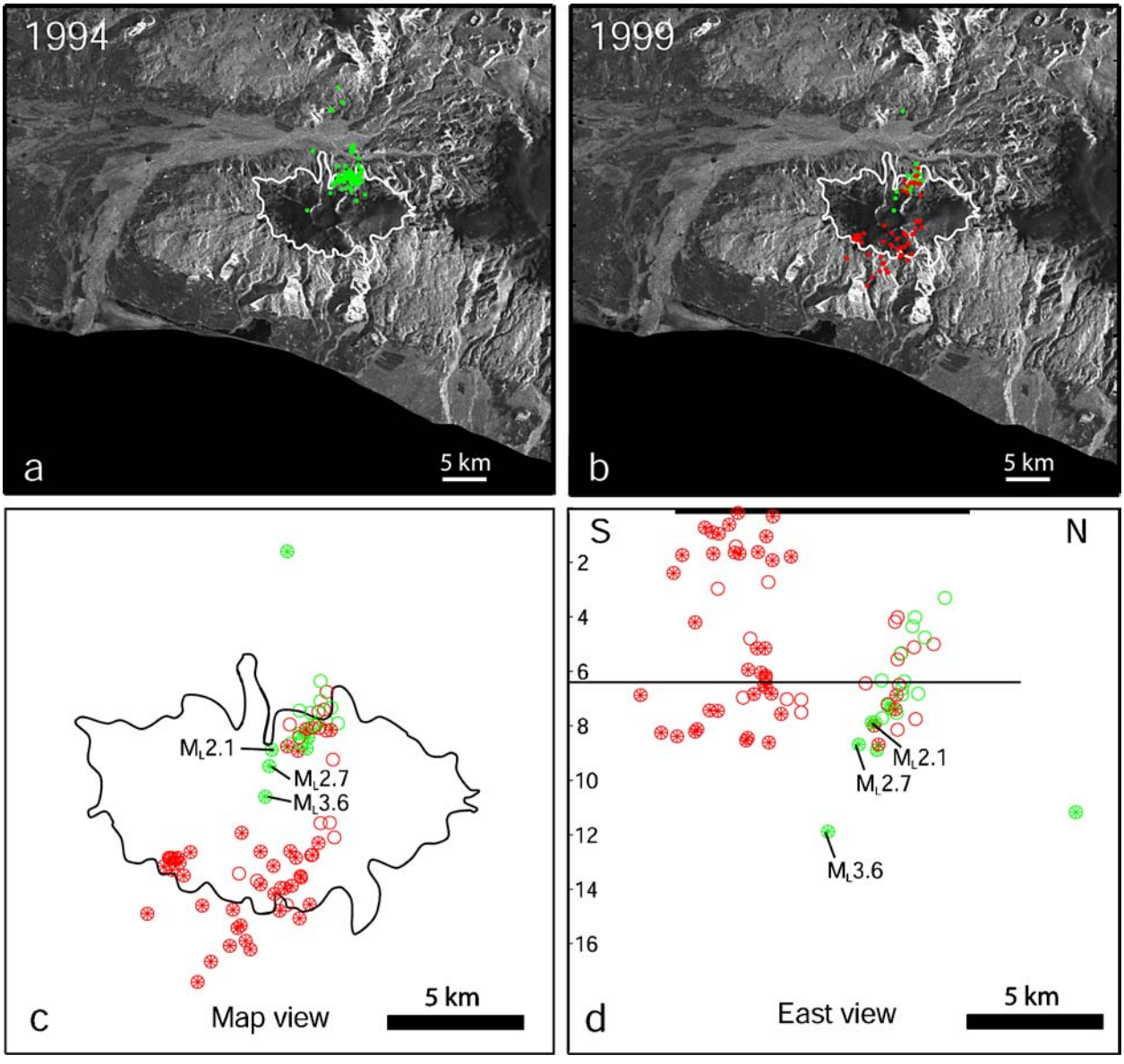

Fig. 2 **a** Earthquake locations for events in 1994 (erz<3.0 km); **b** Earthquake locations for events in 1999 (erz<3.0 km). Green events occurred from January through June. Red events occurred from July through December. The *white line* marks the glacier boundary. **c** Earthquake locations from 1999 having estimated rms travel-time residuals ≤0.2 s, horizontal error (erh)≤1.5 km, and largest gap between recording stations ≤180°. *Star filled circles* mark "well located" events having erz<2.0 km. *Open circles* have erz<3.0 km. Same color code as in panel b. **d** Vertical N–S cross-section, showing the depth distribution for 1999 earthquakes. Same color code and symbols as in panel c. The *black line at the surface* marks the extent of the glacial cover. *Black line at depth* marks the extent of the modeled sill plane. Earthquake locations were kindly provided by the IMO (SIL database 2004)

earthquake had a magnitude of M_L=2.5, and of the 120 recorded events in the swarm, 52 were of of a local magnitude of 1.2 and larger. The swarm activity included a 2-month period of relatively low activity from mid-September to mid-November, which divided the swarm into a main seismic period before the activity, and a secondary seismic period after it. Through all of 1999, a total of 165 earthquakes ($M_L \leq 3.6$) were recorded in the Eyjafjallajökull area (Fig. 2b). The earthquake detection limit for the SIL network was unchanged from 1994. Revised SIL earthquake locations were provided by Kristín Vogfjörd, Icelandic Meteorological Office (personal communication 2004).

The largest seismic moment release in 1999 within the Eyjafjallajökull area occurred before the swarm and crustal deformation (Sturkell et al. 2003). The total seismic moment for 1999 was about 36×10^{12} nm, of which 85% was released before the swarm activity and crustal deformation started. The moment release is dominated by a M_L3.6 event at 11.8 km depth on March 1, followed on May 3 by a M_L2.7 and a M_L 2.1 at 8.6 and 7.8 km depth, respectively (Fig. 2c and d).

Crustal deformation resulting from the 1999 intrusion was measured by dry-tilt and network GPS measurements. These bracketed the deformation as starting between July

19 and August 20, 1999 and ending between February and May 2000. Sturkell et al. (2003) interpreted the deformation as being caused by an inflating Mogi point source at a depth of 3.5±0.6 km situated beneath the southern slopes of Eyjafjallajökull, similar to the 1994 event. The limited GPS and tilt data spanning the 1994 event are, however, not sufficient to constrain a source depth for that event.

Interferometric data

InSAR imaging is becoming an important tool for measuring surface deformation at Icelandic volcanoes (e.g., Sigmundsson et al. 1997a; Feigl et al. 2000; de Zeeuw-van Dalfsen et al. 2004; Pedersen and Sigmundsson 2004). In this study, we used InSAR images to study ground displacements resulting from the 1999 Eyjafjallajökull intrusive event. All radar images were acquired by the ERS-1 and ERS-2 satellites. Data from two adjacent, descending track frames were utilized, but no favorable image combinations from ascending tracks were available. Incidence angles vary from 19 to 27 ° across each ~100-km-wide scene. Image processing was done using the PRISME/DIAPASON software (CNES 1997) in the two-pass approach (Massonnet and Feigl 1998). Digital elevation modeling (DEM), orbital modeling, and filtering have all been previously described (Feigl et al. 2000).

In total, 52 interferograms were processed that covered the study area, spanning the years 1992–2000. Of these, 29 interferograms were from ERS track 324 and 23 from ERS track 52 (Table 1). InSAR images displaying deformation originating from the 1994 intrusion were studied by Pedersen and Sigmundsson (2004). No deformation was detected in the inter-intrusive period from 1995 through 1998 (Fig. 3). Based on time-spans and data quality (depending on image coherence, atmospheric noise level, and baseline separation), nine images were selected for examinations of the deformation field created by the 1999 intrusive episode (Fig. 4, Table 2). All images used in the inverse modeling have an altitude of ambiguity (h_a) above 100 m (Table 2). The h_a is related to the orbital separation between image acquisitions, and equals the size of a DEM error that would produce one artifactual color fringe. With h_a values above 100 m and a DEM with an estimated vertical accuracy of about 30 m, we can discard the presence of topographic fringes in our data. The nine images span various parts of the main seismic period (Fig. 4) and were divided into five time-span groups for the modeling procedure (Table 2). Three groups include just one image, but the division is convenient when explaining the time-dependence of the deformation. Group A consists of four independent images spanning the entire intrusion. The interferometric fringes document that more than 20 cm of range change in the satellites line of sight (LOS) did occur, with the apparent center of deformation being just south of the glacier rim. Five additional interferograms cover different time spans of the intrusive episode. Group B covers the beginning (until Aug. 6) of the assumed main intrusion period. Two deformational fringes are seen just south of the glacier rim.

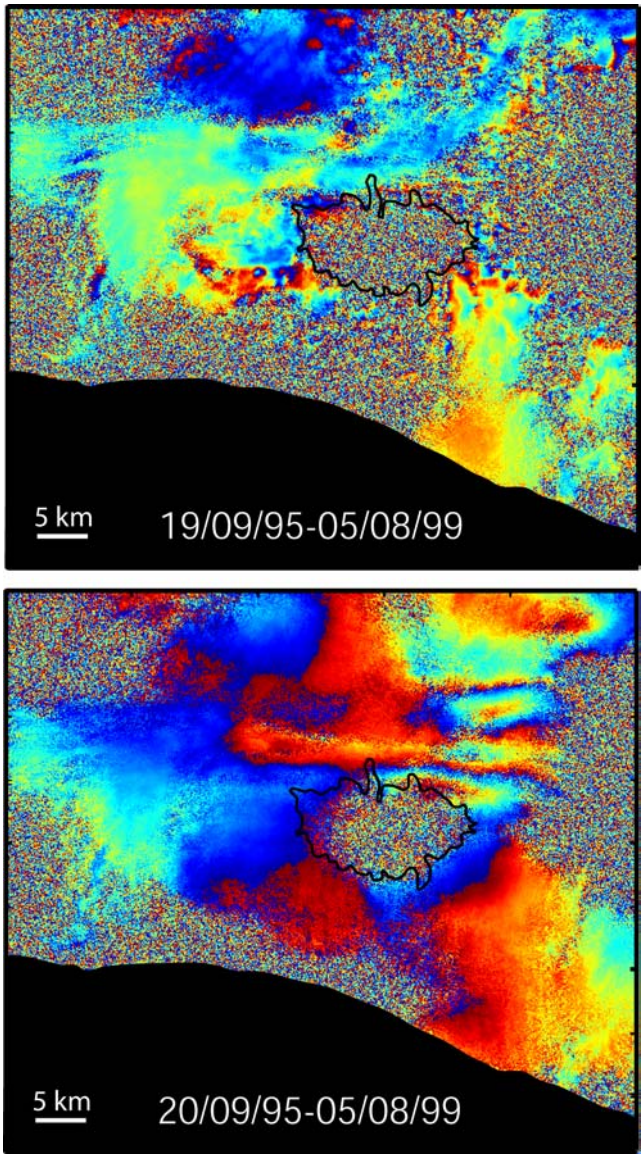

Fig. 3 Two inter-intrusive interferograms showing that no deformation occurred in the Eyjafjallajökull area during the period from September 1995 to August 1998. The fringes seen to the northeast of the glacier rim on the top image can, from pair-wise logic, be identified as atmospheric disturbances

Group C spans an additional 19 days of the intrusion (until Aug. 25) and up to four fringes are seen. Group D spans further 51 days (until Oct. 15), and displays up to six fringes of deformation. The two interferograms in Group D share their slave image, hence they are not independent. Severe atmospheric disturbances are seen in these just north of the Eyjafjallajökull volcano. Finally, Group E records the deformation created after Aug. 25 via the slave image from Group C as a master image, hence Group C and E are not independent datasets. This image displays three deformational fringes.

The presence of atmospheric artifacts in our deformation data may have an effect on the source modeling, depending on the intensity of the noise. When trying to estimate the source responsible for subtle deformation signals, the

Table 1 List of interferograms

Track	Master date			Slave date			M.orbits	S. orbits	h_a (m)
52	1993	AUG	3	1996	SEP	20	−10718	7421	−142
52	1993	AUG	3	1997	JUN	27	−10718	11429	473
52	1993	AUG	3	1997	JUL	31	−10718	−31603	−213
52	1993	AUG	3	1997	AUG	1	−10718	11930	−139
52	1993	AUG	3	2000	SEP	29	−10718	28463	−202
52	1996	SEP	20	1997	JUN	27	7421	11429	109
52	1996	SEP	20	1997	AUG	1	7421	11930	−6893
52	1996	SEP	20	2000	SEP	29	7421	28463	473
52	1997	JUN	27	1997	JUL	31	11429	31603	304
52	1997	JUN	27	1997	AUG	1	11429	11930	−107
52	1997	JUN	27	1999	OCT	15	11429	23453	243
52	1997	JUN	27	2000	SEP	29	11429	28463	−142
52	1997	JUL	31	1999	OCT	15	31603	23453	610
52	1997	AUG	1	2000	SEP	29	11930	28463	442
52	1997	SEP	5	1999	AUG	6	12431	22451	−1030
52	1998	JUL	17	1998	AUG	21	16940	17441	−48
52	1998	JUL	17	2000	JUN	16	16940	26960	−53
52	1998	JUL	17	2000	JUL	21	16940	27461	−214
52	1998	AUG	21	2000	JUN	16	17441	26960	455
52	1998	AUG	21	2000	JUL	21	17441	27461	61
52	1999	MAY	28	1999	AUG	6	21449	22451	−72
52	1999	OCT	15	2000	SEP	29	23453	28463	−76
52	2000	JUN	16	2000	JUL	21	26960	27461	71
324	1992	AUG	2	1995	JUN	6	−5479	−20352	−352
324	1992	AUG	2	1995	SEP	20	−5479	2182	106
324	1992	AUG	2	1998	AUG	5	−5479	17212	104
324	1992	AUG	2	1998	SEP	9	−5479	17713	−57
324	1992	AUG	2	1999	JUN	16	−5479	21721	−942
324	1992	SEP	6	1995	AUG	15	−5980	−21354	1150
324	1992	SEP	6	1995	AUG	16	−5980	1681	204
324	1992	SEP	6	1999	SEP	29	−5980	23224	88
324	1995	JUN	6	1995	SEP	20	−20352	2182	82
324	1995	JUN	6	1998	AUG	5	−20352	17212	80
324	1995	JUN	6	1998	SEP	9	−20352	17713	−68
324	1995	JUN	6	1999	JUN	16	−20352	21721	562
324	1995	AUG	15	1995	AUG	16	−21354	1681	248
324	1995	AUG	15	1999	SEP	29	−21354	23224	96
324	1995	AUG	16	1999	SEP	29	1681	23224	156
324	1995	SEP	19	1998	AUG	5	−21855	17212	106
324	1995	SEP	20	1998	AUG	5	2182	17212	5733
324	1995	SEP	20	1999	JUN	16	2182	21721	−95
324	1995	SEP	20	2000	SEP	13	2182	28234	64
324	1998	JUL	1	1999	AUG	25	16711	22723	−185
324	1998	JUL	1	2000	MAY	31	16711	26731	−77
324	1998	AUG	5	1999	JUN	16	17212	21721	−94
324	1998	AUG	5	2000	SEP	13	17212	28234	65
324	1998	SEP	9	1999	JUN	16	17713	21721	60
324	1998	SEP	9	1999	SEP	29	17713	23224	−62
324	1998	SEP	9	2000	AUG	9	17713	27733	164
324	1999	JUN	16	2000	AUG	9	21721	27733	−95
324	1999	AUG	25	2000	MAY	31	22723	26731	−131
324	2000	MAY	31	2000	SEP	13	26731	28234	−41

Negative orbit numbers are from ERS-1; positive orbit numbers are from ERS-2

Table 2 Interferograms used for modeling

Group	Image No	Master orbit	Slave orbit	Track	Master date	Slave date	h_a (m)	Reduced data size
A	1	17713	27733	324	09/09/98	09/08/00	164	300
	2	11930	28463	52	01/08/97	29/09/00	442	317
	3	16940	27461	52	17/07/98	21/07/00	–213	338
	4	17441	26960	52	21/08/98	16/06/00	455	295
B	5	12431	22451	52	05/09/97	06/08/99	–1030	100
C	6	16711	22723	324	01/07/98	25/08/99	–185	214
D	7	31603	23453	52	31/07/97	15/10/99	610	306
	8	11429	23453	52	27/06/97	15/10/99	243	134
E	9	22723	26731	324	25/08/99	31/05/00	–131	229

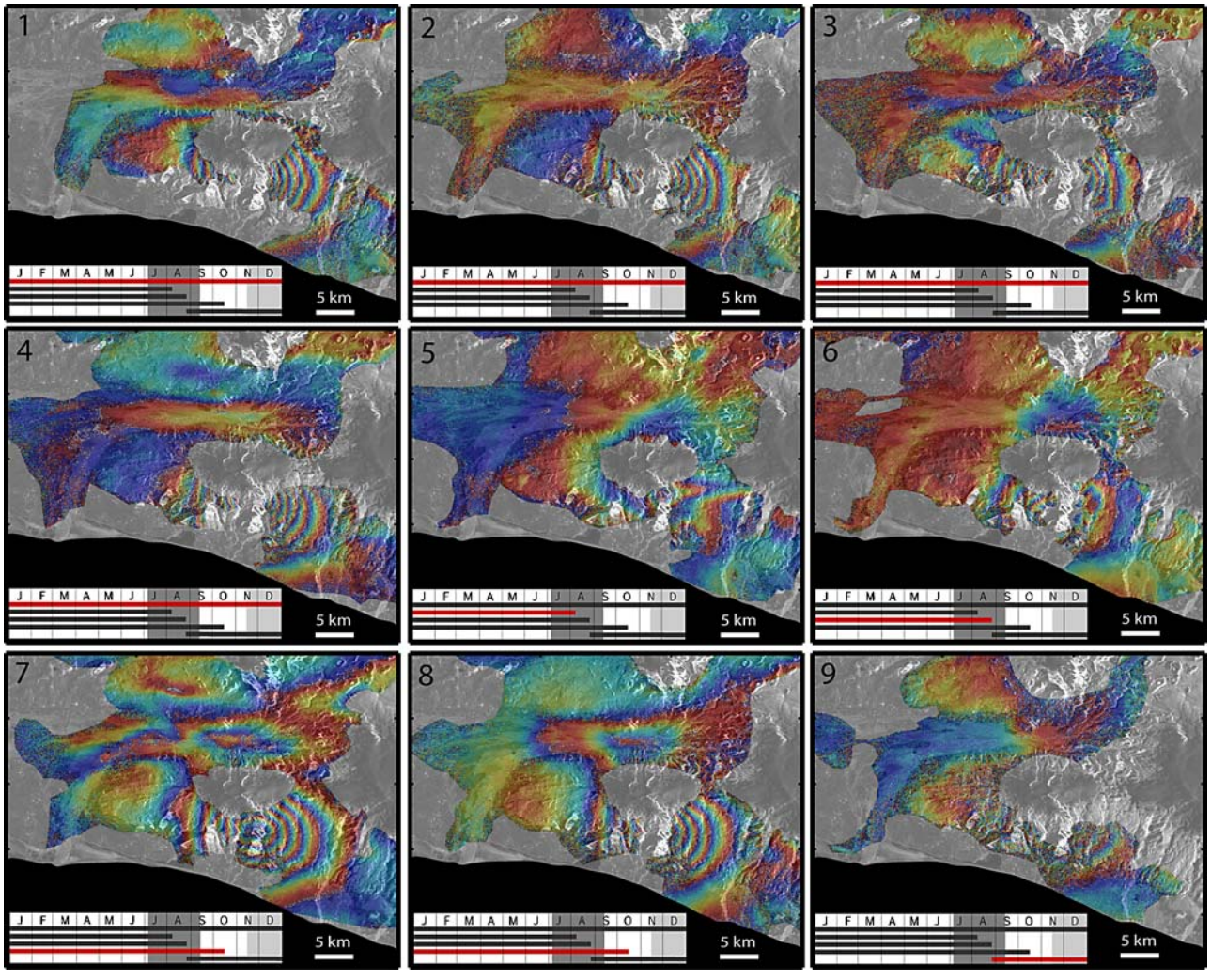

Fig. 4 The nine interferograms selected for modeling the 1999 intrusive episode. Incoherent areas are *masked*. Amplitude image *in background*. The area corresponds to Fig. 1b. The time span *insets* show the relation to the period(s) of elevated seismic activity (*Dark gray* main seismic period; *Light gray* secondary seismic period). The interferograms spans 2–3 years, but only the 1999 period is displayed. For details on dates please refer to Table 2. One *full color cycle* corresponds to a change in range of 2.8 cm

model is more susceptible to atmospheric noise, due to the low signal-to-noise ratio in these cases. However, if several independent interferograms are used for estimating the deformation source model, the effect from atmospheric artifacts in the dataset is suppressed.

All interferograms were unwrapped using Markov Random field regularization and a simulated annealing optimization (Gudmundsson et al. 2002). The number of InSAR data points was reduced by quadtree partitioning, a two-dimensional quantization algorithm (e.g., Welstead

1999). The quadtree data are used as the input data in subsequent inverse modeling in order to speed up model computations. The reduced data size (Table 2) in combination with an assigned uncertainty of 5–10 mm, based on altitude of ambiguity and atmospheric noise level, is used to weight the data in model calculations.

Modeling approach

To visualize the subsurface source of the deformation recorded in our dataset, we need to create a model based on some simplifying assumptions. Rocks surrounding a deformation source at depth act as low-pass filters on the details of the source, and therefore simple source geometries such as point sources or plane sheets adequately simulate deformation recorded at the surface (Dvorak and Dzurisin 1997). We use the standard approach of assuming that the earth's response can be effectively simulated by that of a homogeneous, isotropic, elastic half-space. We use a Poisson's ratio of ν=0.25. The use of an elastic approach within a volcanically active setting is justified by the lack of convincing evidence regarding the existence of a shallow magma chamber in the Eyjafjallajökull volcanic system.

We apply an inversion procedure to derive the deformation source. To obtain maximum robustness, we first apply a simulated annealing algorithm subsequently followed by a derivative-based method, as recommended by Cervelli et al. (2001) and used, e.g., in Pedersen et al. (2003). For interferometric model simulations, we use constant look angles estimated at the center of the area of interest. The unit vector pointing from the ground towards the satellite is given as east, north and vertical components, and has the values 0.394, −0.109, 0.913 for track 52 and 0.355, −0.103, 0.929 for track 324.

GPS vectors from Sturkell et al. (2003) spanning the entire intrusive event were used to evaluate our InSAR derived models. GPS station locations are shown in Fig. 1b. Given the limited GPS data set (six stations) which provides only a few constraints on the temporal evolution of the sill intrusion, we did not use the data in the inversion procedure. The GPS measurements, however, have the advantage of supplying information about the three-dimensional deformation field, whereas InSAR data only supplies a one-dimensional measurement in the LOS direction. GPS measurements, therefore, have the potential of providing constraints on the most likely geometry of the magmatic source, as point sources, dikes and sills result in different deformation patterns at the surface. Measurements are, however, required to cover both near-field and far-field deformation, with respect to the source, in order to clearly distinguish between model responses (Dzurisin 2003).

Point source modeling

Mogi point source modeling (Mogi 1958) is the simplest approach to simulate volcano deformation. The model consists of only four parameters, defining the coordinates of a point source pressure and a volume change. It has been used extensively in volcano deformation studies (Table, p. 363 in Dvorak and Dzurisin 1997; Massonnet and Sigmundsson 2000; Amelung et al. 2000; Feigl et al. 2000; Pritchard and Simons 2002; Lu et al. 2003).

We initially tested the model based on GPS and tilt measurements presented by Sturkell et al. (2003) on our InSAR data. Next, two approaches were undertaken for point-source optimization of the InSAR data. First, all parameters were optimized for each data group individually. Subsequently, the inversion was carried out with the Mogi source depth fixed at the optimal value found by inversion of Group A interferograms spanning all of 1999.

Plane source modeling

A more advanced source geometry for volcano deformation modeling is the dilatational sheet model by Okada (1985). This model is also commonly used for volcano deformation studies (e.g., Okada and Yamamoto 1991; Linde et al. 1993; Jónsson et al. 1999; Amelung et al. 2000). Eight model parameters define the source geometry and location (x and y location, length, width, depth, dip, strike and opening). We initially left all parameters unconstrained, thereby allowing for both dike and sill simulation. A dike model is not capable of reproducing the deformation pattern observed. For all models, the dip showed less than 2° deviation from horizontal and the plane was subsequently fixed to horizontal. A two-step inversion procedure was used for estimating the variable opening of the sill model. First, exhaustive searches for the best-fit model parameters of a uniform opening sill were carried out. The model parameters describing the geometry were subsequently fixed at the optimal values. We then divided the plane into patches of 1×1 km in size, and estimated the opening on each, thereby allowing for spatial variations in the sill thickness. The horizontal dimensions were expanded to allow for tapering of sill opening at the boundaries. The approach is the same as used by Amelung et al. (2000). Without using an appropriate amount of smoothing, we obtained a solution with irregular opening values on adjacent patches. Such an opening model may give the best fit to the data, but is unrealistic. To obtain a non-oscillatory sill-opening, we applied a smoothing constraint, which minimizes the second-order spatial derivative (Laplacian) of the opening (e.g., Jónsson et al. 2002).

Modeling results

For a null model, i.e., without optimizing any deformation source model, the weighted total residual mean square (RMS) for Group A interferograms is 6.9 cm. A Mogi source fixed at 3.5 km depth suggested by Sturkell et al. (2003) only decreases the Group A RMS to 2.1 cm. This model does not fit the InSAR data well, as up to five fringes occur in residual interferograms. When optimizing all model parameters of a Mogi point source, the Group

Table 3 Inversion results

Group	Image No	Data weight	Null model	Mogi				Variable Opening Sill[a]			
				Variable depth[b]		Fixed depth[c]		Stationary steps		Time progressive	
			RMS (cm)	Total volume (km^3)	RMS (cm)	Total volume (km^3)	RMS (cm)	Total volume (km^3)	RMS (cm)	Total volume (km^3)	RMS (cm)
A	1	24%	6.4	0.036	1.6	0.036	1.6	0.029[d]	0.9	NA[e]	NA
	2	25%	7.6		1.4		1.4		0.9		NA
	3	27%	6.1		1.3		1.3		1.1		NA
	4	24%	7.6		1.1		1.1		0.7		NA
B	5	100%	2.0	0.010	0.7	0.011	0.7	0.008	0.6	0.008	0.6
C	5	100%	4.3	0.018	0.7	0.020	0.8	0.015	0.7	0.018	0.8
D	7	53%	5.7	0.026	0.9	0.025	1.0	0.025	0.6	0.025	0.9
	8	47%	5.1		0.6		0.6		0.4		0.8
E	9	100%	3.4	0.033	1.1	0.037	1.1	0.028[f]	0.9	0.031[g]	1.3
Volume discrepancy[h]		0.003		−0.001		0.001		−0.002			

[a]Fixed depth at 6.3 km (see Fig. 6)

[b]Depth of 6.1, 5.8, 5.6, 5.9, and 4.3 km for Group A–E, respectively

[c]Depth of 6.1 km

[d]Total volume of S1 model

[e]Not applicable

[f]Total volume of S2 model estimated as $Vol_{Group\ C}+Vol_{Group\ E}$

[g]Total accumulated volume of S3 model estimated as $Vol_{Group\ B}+Vol_{Group\ C}+Vol_{Group\ D}+Vol_{Group\ E}$

[h]Difference between volume estimate for Group A and the stepwise accumulated total volume estimate

A data RMS reduces to 1.3 cm. Then the optimal depth for Group A data is 6.1 km, while for Group B–E the source depth varies between 4.3 and 5.9 km. Volume estimates and RMS values for Group A–E are shown in Table 3. A discrepancy of 0.003 km^3 exists between the accumulated total intrusion volume estimated from adding the volumes found for Group C and E and the volume estimate from optimizing Group A. In a second approach, model calculations for all data groups are based on a fixed source depth of 6.1 km, which reduces the estimated volume discrepancy to −0.001 km^3. Surface projected locations with error estimates of 1 SD for these five Mogi sources are shown in Fig. 5. It is evident from the modeling that a point source model does not adequately simulate the total deformation measured by InSAR.

A simple test of the InSAR resolvable depth of magma extraction showed that for the emplacement of 0.036 km^3 of magma at 6.1 km depth, and extraction of an equal volume at greater depth, the magma must originate from a source located deeper than about 17 km below the surface, assuming a deformation detection threshold of 10 mm. If it is located beyond this level, and when superimposed on the uplift signal created by the shallow intrusion, we are unable to resolve surface deformation resulting from extraction of magma.

A sill model provides a significantly improved fit compared to the Mogi model for Group A interferograms. The optimal intrusion depth for a uniform opening sill was found to be 6.3 km, based on multiple runs of the inversion procedure, varying the depth and optimizing all other parameters (Fig. 6). A uniform opening sill model with a thickness of 0.51 m and a volume of 0.029 km^3, reduces the weighted total Group A RMS to 0.9 cm. By allowing the opening to vary, the RMS is unchanged, but the procedure of estimating variable opening is essential for investigation of the spatio-temporal evolution of the sill. The maximum sill thickness is then 0.92 m with unchanged total intrusion volume. This solution, henceforth termed S1, is shown in Fig. 7a. Figure 8 shows an example of data, simulated interferograms from the S1 model and the resulting residual.

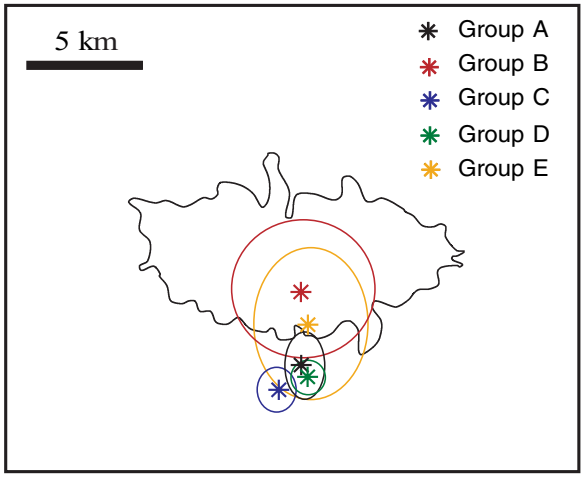

Fig. 5 Optimal Mogi source locations for the five data groups. Calculations are based on a fixed source depth of 6.1 km. *Ellipse axes* show error estimates of 1 SD error for latitude and longitude of source location. *Black line* outlines the Eyjafjallajökull glacier

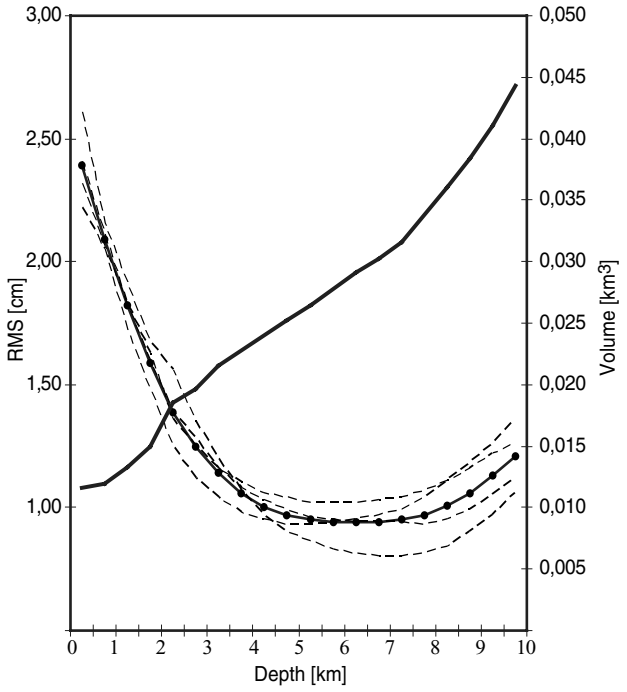

Fig. 6 Optimal depth estimation for a sill intrusion. *Solid black line* shows the volume, *dotted line* shows total RMS, and *stippled lines* are RMS values for individual Group A interferograms

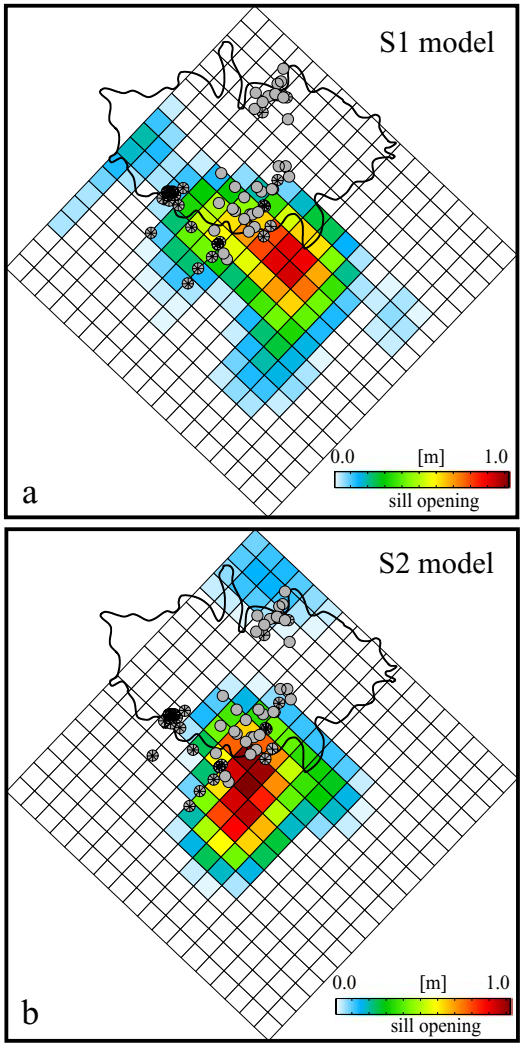

Fig. 7 **a** Sill model S1. Variable opening estimated from inversion of Group A igrams (total intrusion). Earthquakes occurring between July and December are shown. Well-located earthquakes have *black star fillings*. **b** Sill model S2. Total variable opening estimated from Group C + Group E optimizations. Earthquakes as in panel a

Next, we aim to estimate the spatio-temporal evolution of the sill. Modeling was done using two different approaches, both based on the sill geometry found by inversion of Group A data. First, we solve for the optimal variable sill-opening model for each of the four time intervals represented by Group B–E. The variable opening sill solutions contain small patches of minor opening disconnected from the main sill. These patches are attributed to noise in the data and are manually removed from the solutions before calculating the resulting RMS and volume estimates (Table 3). A cluster of opening patches coinciding with the earthquakes on the northern slopes of the volcano appear in individual optimizations for both Group B and Group C data. The patches were not removed from the models as it was considered unlikely that they were caused by atmospheric noise (discussed further below). By combining the sill openings obtained from inversion of Group C and E, we obtain a model (S2) for the entire time span of the intrusion (Fig. 7b), having a total volume of 0.028 km^3.

In our second approach, we seek to resolve the spatio-temporal evolution of the sill in greater detail, utilizing the different time spans of the interferograms and requiring the deformation to be time-progressive. First, we optimize Group B for a variable opening sill and clean out the minor patches of opening attributed to noise in the data (Fig. 9a). We then subtract the resulting deformation from Group C data, optimize the modified data, and again clean out the opening attributed to noise. The total deformation resulting from the combined models for Group B and modified Group C (Fig. 9b) is then subtracted from Group D and again the modified data are optimized. The total sill opening after this step is shown in Fig. 9c. Finally, for Group E, we subtract the deformation predicted by the optimization of the modified Group D data, and invert for a model representing the final stage of the intrusion. However, the signal-to-noise ratio is low for this dataset (Fig. 4, panel 9) and the time-dependant modeling is not optimal, as seen by the resulting RMS of 1.3 cm. The four-step time-dependant sill evolution is shown in Fig. 9 with the resultant model (S3; Fig. 9d). This model gives a total intrusion volume of 0.031 km^3.

Discussion

Comparison of modeling approaches

Based on GPS measurements Sturkell et al. (2003) suggested that the 1999 deformation field could be fitted by a Mogi point source at 3.5±0.6 km depth. Our InSAR-based inversion result with a point source fixed at this depth gives

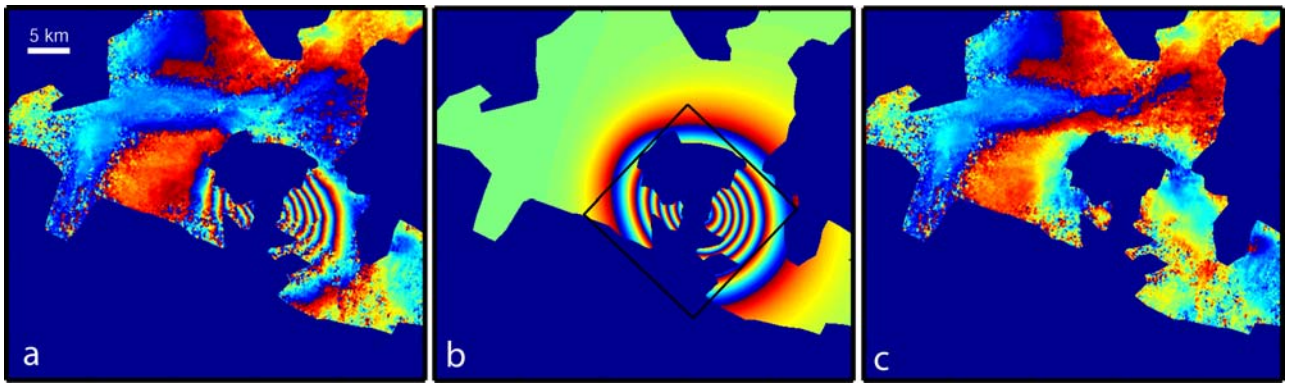

Fig. 8 **a** Interferogram 2 in Fig. 4; **b** simulated interferogram from model S1; Black line shows outline of the modeled sill plane shown in figure 7a **c** residual interferogram after model subtraction

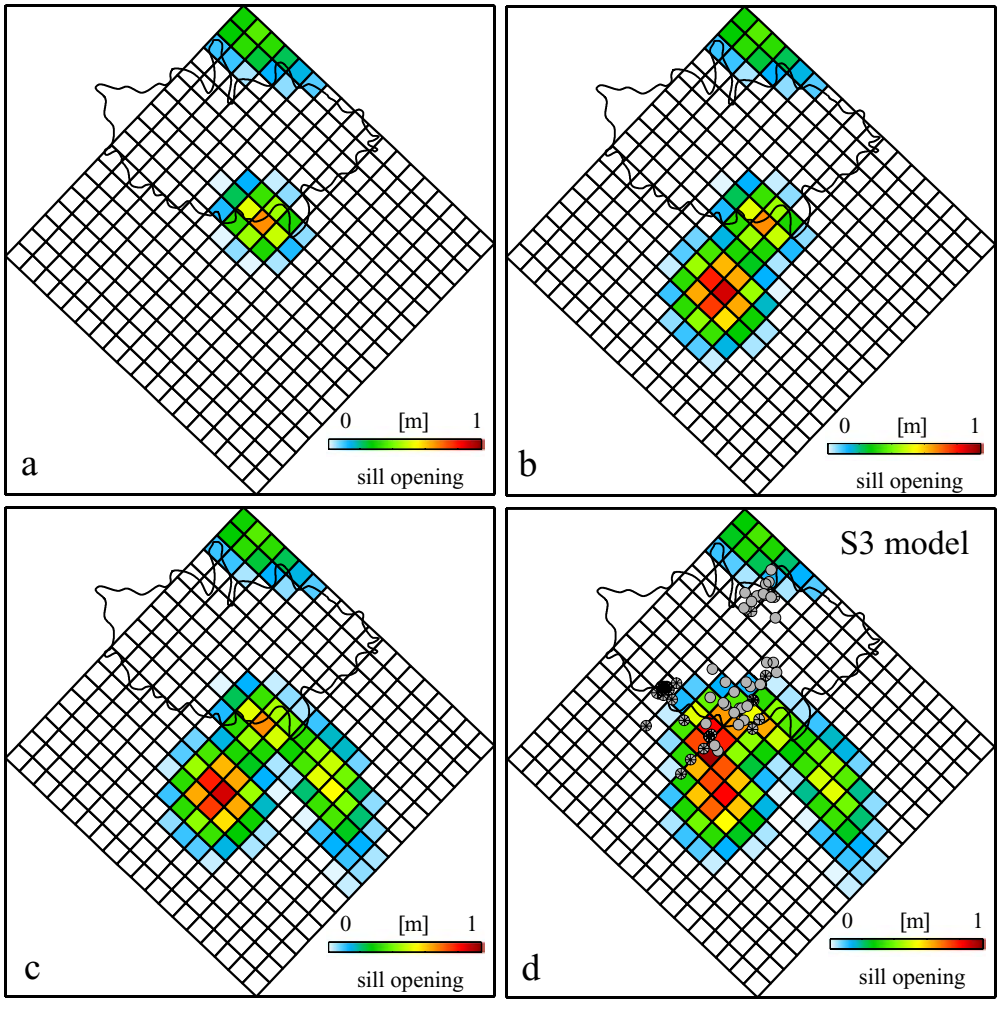

Fig. 9 Time-progressive variable sill opening model S3. **a** Until August 6; **b** until August 25; **c** until October 15; **d** total opening. Earthquakes occurring between July and December are shown. Well-located earthquakes have *black star fillings*

a volume estimate of 0.018 km^3, similar to the estimate from GPS data (0.017 km^3), but the model does not provide a good fit to the InSAR observations. A deeper more voluminous source is strongly favored by our data (Table 3).

The two modeling approaches taken here to explain the observed deformation by expanding the Mogi point sources result in volume estimates between 0.033 and 0.037 km^3. The source locations shift vertically up to 1.8 km and horizontally up to 5.0 km N–S and 1.5 km E–W in the variable depth models. If the deformation recorded in the interferograms were due to injection of magma into an existing chamber, we would expect the center of deformation to remain constant through time. In addition, the inversion results based on the data covering the whole period of the

intrusion (A in Table 3) gives a relatively high RMS compared to what is obtained for independent inversion of data covering shorter time spans (B–E in Table 3). The variations in the Mogi source location for individual short time spans combined with the high RMS value for Group A indicates that the source of the deformation migrated through the duration of the intrusion. We interpret this as an indication that more complex source geometry is needed to explain the measured ground deformation. We, therefore, prefer a sill geometry rather than a point source model.

Another argument against the deformation originating from a spherical intrusion is the overpressure required. For a cold structure like the Eyjafjallajökull volcano (with no residing magma chamber), the pressure required to create a point source is on the order of 40 GPa, as

$$\Delta P_{\text{point}} = 4\mu/3, \tag{1}$$

where μ is the shear modulus, here set to 30 GPa (Sigmundsson 1996). The tensile strength of the Icelandic crust is not well known, but analysis of hydrofracturing measurements have revealed it to be on the order of 1–6 MPa (Haimson and Rummel 1982), implying that the pressure required to produce a point source exceeds the tensile strength of the elastic host rock by more than four orders of magnitude. A horizontal, plane circular sheet intrusion similar to the ones in this study only requires an overpressure on the order of 4 MPa to form, as

$$\Delta P_{\text{sheet}} \approx \mu \times u/\left((1-\nu)\right) \times L\right), \tag{2}$$

where u is the sheet thickness, L the radius and ν the Poisson's ratio of the host rock (Lister and Kerr 1991).

For the sill modeling, three variable opening solutions were produced through the different approaches taken. Volume estimates vary between 0.028 and 0.031 km^3. The relatively low variation in volume indicates that our modeling approaches are robust. The three different variable opening sill models all result in similar opening and horizontal dimensions, but some deviations are seen between models. The S2 and S3 solutions (Figs. 7b and 9d) are obtained without any reference to Group A data. To evaluate their credibility, we then tested them on Group A data with the resulting RMS values amounting to 1.9 and 1.5 cm, respectively. These values are admittedly higher than for S1, which was optimized for the Group A dataset. The S2 and S3 models do, however, account for 72% and 79% of the signal in Group A respectively, compared to 87% for S1 (calculated as $(\text{RMS}_{\text{Null}} - \text{RMS}_{\text{Residual}})/\text{RMS}_{\text{Null}} \times 100$). For the temporal evolution, we prefer the S2 model since individual optimizations are not influenced by previous estimates of sill opening as in the S3 model.

A significant feature present in both the S2 and S3 models is the cluster of opening patches seen in the area just north of the glacier rim (Figs. 7b and 9d) where most earthquakes occurred before and after the main deformation period (discussed further in the next section). The opening is related to a subtle deformation signal present north of the glacier rim in the independent Group B and C data. Because of the close resemblance between the signals in Group B and C data, we interpret the signal to be real, and not attributed to atmospheric noise. We suggest that the area of high earthquake activity (discussed further in the next section) may be the site of a feeder channel supplying magma to the sill intrusion. The magma spreads horizontally towards the south. We do not imply that our modeling accurately reproduces the source of the observed deformation signal on the northern slopes of the volcano, but merely indicate that some process linked to the feeder channel caused subtle surface deformation. The reason that a signal related to a possible feeder dike does not appear in other data may be the following: Group A and D data suffer from moderate to severe atmospheric disturbances in this particular area. However, there may be an indication of a similar signal in Group A, interferogram 2 (Fig. 4, Panel 2); Group E data span only the final phase of the intrusion and deformation may already have terminated in that area. We have not attempted to further investigate the signal as it is very small (∼2 cm in the LOS direction) and only limited interferometric data are available due to the proximity of the glacier. If the feeder channel is indeed located close to the northern rim of the glacier, the question then arises as to why the opening patch is isolated from the main sill opening in all three models. An obvious potential explanation is the lack of deformation data within this area due to the ice cap cover. Resolution tests performed on synthetic data with added noise reveal that small sill opening in the area beneath the glacial cover will appear in models as disconnected patches of sill opening north and south of the glacier (Fig. 10). However, the resulting volume estimate appears to be robust, and deviates less than 3% from the input.

A significant difference between the S3 model compared to both S1 and S2 is the opening lobe towards the southeast. The opening is found by optimizing a dataset where two previous deformation models, which may have been affected by various degrees of small-scale data noise, have been subtracted. Therefore, this particular time-step optimization may be of less quality compared to the others, where no or only one prior model step has been subtracted. The result of the third step optimization in the S3 modeling approach (Fig. 9) is the model with which we modify Group E data. It may carry errors into the last step of the optimization and cause problems in obtaining a good model for the final phase of the deformation. Despite its limitations, our time-dependant sill evolution model (S3) provides a basic explanation for the migration of the center of deformation through the evolution of the intrusion.

Measured GPS displacements and calculated model predictions from three of the above-mentioned models are shown in Fig. 11. The model responses considered are a Mogi point source inverted to fit the InSAR data and fixed at 3.5 km depth (M1), a Mogi point source fixed at 6.1 km (M2), and our S1 sill model. All sill model responses were tested, but only S1 predictions are plotted for clarity, as they produce relatively similar results. The largest GPS displacements, for both the horizontal and vertical components, are seen at station SELJ. Our S1 model fits the vertical component slightly better than the M1

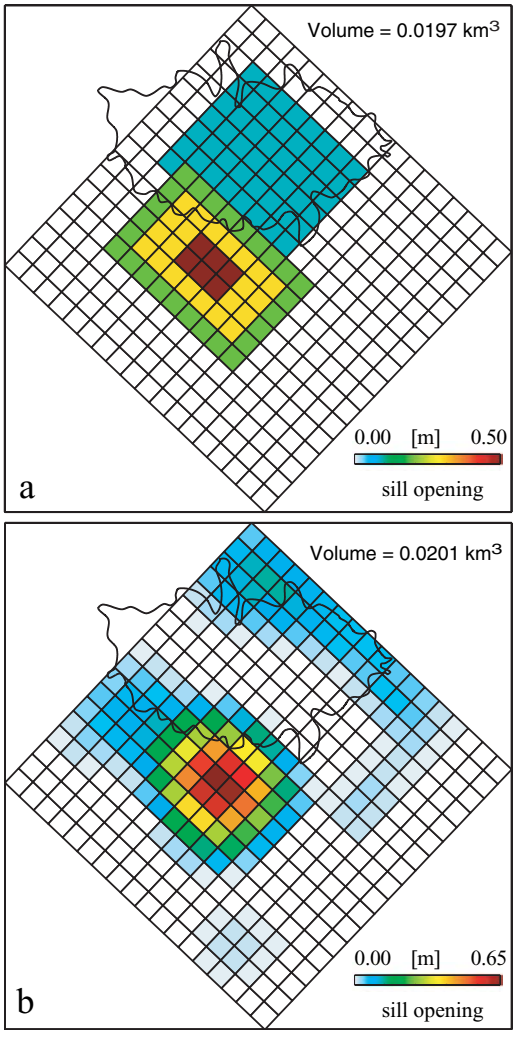

Fig. 10 Resolution test results. Note the difference in color scales. **a** Sill model used to create a synthetic dataset. Noise was added to the data before running the inversion code. **b** Resultant sill model. The area of low sill opening beneath the glacial cover is resolved as disconnected opening patches to the north and south of the glacier. The volume estimate is however robust to within 3%

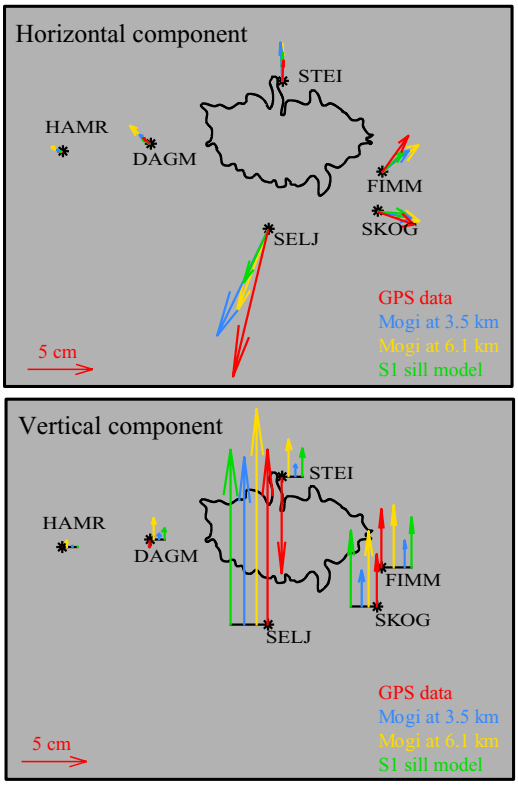

Fig.11 GPS measurements from Sturkell et al. (2003) and model predictions calculated for the S1 sill model and point source models at depths of 3.5 and 6.1 km. GPS displacements span July 1998 to July 2000

model. However, the horizontal component at this station is not well predicted by any of the models. The M1 model provides the smallest residual, as the large horizontal displacement is best explained by a shallow source. The horizontal residual at SELJ does, however, still amount to more than 3 cm. It is noteworthy that this residual horizontal displacement is directed seawards away from the volcano flank. A possible role of slope or even flank instability is suggested. However, a more extensive GPS coverage would be needed to resolve it if such processes are taking place. The seaward motion may go undetected in InSAR images as the technique is least sensitive to N–S movements. A 3-cm displacement directed due south would result in only 0.3 cm of range change in the InSAR image giving only one tenth of a fringe. For other GPS stations than SELJ, there is no conclusive evidence of one model being superior to another, as the predictions fit to measurements vary between stations. At station STEI, all models predict uplift in agreement with the available InSAR data, but significant subsidence was measured via GPS. Sturkell et al. (2003) suggested that the STEI station may be unstable.

Earthquake activity

For this study, we filtered the available seismic data by selecting only the best located events during all of 1999, based on the following criteria: locations having estimated rms travel-time residuals $\leq$0.2 s; horizontal error (erh)$\leq$1.5 km; vertical error (erz)$\leq$3.0 km; and largest gap between recording stations $\leq$180°, reducing the dataset from 165 to 79 events. Of these, 48 have erz$\leq$2.0 km and are termed "well located." During the first 6 months of 1999, 19 events fulfill our selection criteria, with 7 events being well located. The epicentral locations of these earthquakes generally coincide with the cluster of activity observed at the northern flank of the volcano during 1994 (Fig. 2a and b). The hypocentral distribution of well-located events from the first half of 1999 fall within a tilted narrow lineament, extending from a 12-km depth centered beneath the volcano, shallowing towards the NNE (Fig. 2c and d). Hypocenters from the earthquake swarm in July and August extend from the northern cluster and 10 km southwards at about 6–8 km depth, with most occurring beneath the glacial region (Fig. 2). By August, seismicity reached south of the glacial cover, to the southern slopes of the volcano

where the main activity remained throughout November. The majority of events in October and November occurred at less than 4 km of depth. In December, seismicity shifted back to the northern cluster.

Based on the temporal and spatial distribution of well-located earthquakes combined with our deformation modeling results, we suggest that the northern cluster of earthquake activity, together with the M_L 2.1, 2.7 and 3.6 events, may delineate the site of a narrow, pipe-like magma feeder channel. The individual model optimizations of independent datasets (Group B and C) both predict a small amount of opening coinciding with the earthquake cluster. Our main conclusions are relatively independent of how much sill opening occurred at the northern earthquake cluster. The earthquakes are the primary evidence for an active process in the area, and we expect the actual feeder channel to be associated with only little or no deformation (see below).

A basic feature of the 1999 seismicity at Eyjafjallajökull is its shift southwards which was initiated with the swarm activity in July (Fig. 2). All well-located earthquakes occurring in July and August are found at a depth of 6–8 km. Prior to the onset of the seismic swarm, all well-located earthquakes had been confined below a depth of 6 km in the area, where we suggest a feeder pipe to be located. The southward shift in earthquake activity is interpreted as accompanying the sill formation stage. The seismic events occur, however, in a limited area, compared to the area of predicted sill opening. Earthquake locations correlate with the general area of maximum sill opening predicted by our various sill models, and their limited occurrence may indicate that the failure level is only exceeded where the main opening imposes the largest stress perturbations.

Additional seismic data from a temporary local network of portable seismic stations deployed from 15/9/99 to 23/10/99, show that micro-earthquake activity (mostly about M_L=0) continued throughout the measurement period (67 events located; B. Brandsdóttir, 2004, personal communication), though only 4 events were detected by the SIL network ($0.8<M_L<1.6$). All the 67 events occurred at the southern slopes of the volcano above 7 km depth, most within the uppermost 2 km (Brandsdóttir 2000). It is evident from the two seismic datasets that persistent micro-earthquake activity occurred at a very shallow level within the southern volcano slopes throughout September, October, and November of 1999. This activity also roughly coincides with the area of maximum sill opening (though the sill is much deeper) predicted by our S2 and S3 model. The shallow cluster of micro-earthquake activity may be induced by stresses produced by the main sill opening at depth combined with a lower lithostatic pressure or by stress perturbations in shallow geothermal water systems or fractures. In December 1999, earthquake activity returned to the northern cluster with all the well-located events occurring at depths of more than 6 km. The location of these earthquakes coincides with the suggested feeder channel. These earthquakes may be related to readjustments of stresses, cooling of the feeder or it may be a failed attempt to resume the intrusion.

We suggest that the southward shift in seismicity may originate from the lateral sill propagation enforcing an increase in the stressing rate towards the south. Our model does not predict any connection between the possible site of a feeder channel in the north and the outline of the main sill, which resolution tests show may be due to the lack of data within this area (incoherent due to the ice cap). The pattern of earthquake locations does, however, suggest that such a connection exists (Fig. 2). If the seismicity at deep levels (6–8 km) in the south is thought to correspond to the onset of crustal deformation within this region, then magma reached the area of predicted main sill opening in early August. This is in excellent agreement with our deformation data, as Group B data show two fringes of deformation created before August 6.

The suggested magma feeder channel may also have been the magma supply path during the 1994 intrusive event at Eyjafjallajökull (Fig 2a). Well-located earthquakes in the 1994 northern cluster (Dahm and Brandsdóttir 1997) extend to shallower depths than what is seen for the 1999 event, in agreement with a shallower source depth (4.6 km) for the 1994 sill model (Pedersen and Sigmundsson 2004). As the intrusion in 1994 was explained by a sill model largely coinciding with the location of the 1999 sill, though at a shallower depth, the question arises as to why the early event did not trigger earthquake activity south of the glacier as seen in 1999. We consider two possibilities related to either breaking strength or intrusion rate. The 1994 earthquake deficiency in the southern slopes may be related to a relatively low prevailing stress level prior to the intrusion. The crustal deformation created in 1994 may have elevated the stress level, but not beyond the breaking strength. The deformation created in 1999 may then have increased the stresses sufficiently to exceed the threshold. Another possible explanation is that the occurrence of earthquakes is related to the stressing rate imposed by the intruded magma, similarly as suggested by Toda et al. (2002). At a low rate of magma intrusion and hence low rate of deformation, earthquake magnitudes may be below the detection limit. If propagation and opening of the sill was slower in 1994 than 1999, related to differences in magmatic pressure, stresses under the southern slopes may have been released through seismicity below the detection limit. In the 1999 episode, an indication of this is observed as only the local, more sensitive network recorded earthquakes in the late stage of the intrusion, which is characterized by a lower intrusion rate (see next section). No intrusion rate estimates are, however, available for the 1994 event, but the volume estimates are about half the volumes inferred for 1999 (Pedersen and Sigmundsson 2004). A lower magma pressure for the 1994 intrusion may also be reflected in the lower accumulated moment release that year compared to 1999. The main moment release in 1999 is not related to the crustal deformation, but inferred to be related to the ascent of magma from deeper levels, as the main moment release occurred in the events on March 1 and May 3. These events make up the deeper part of the inferred pipe-like feeder channel

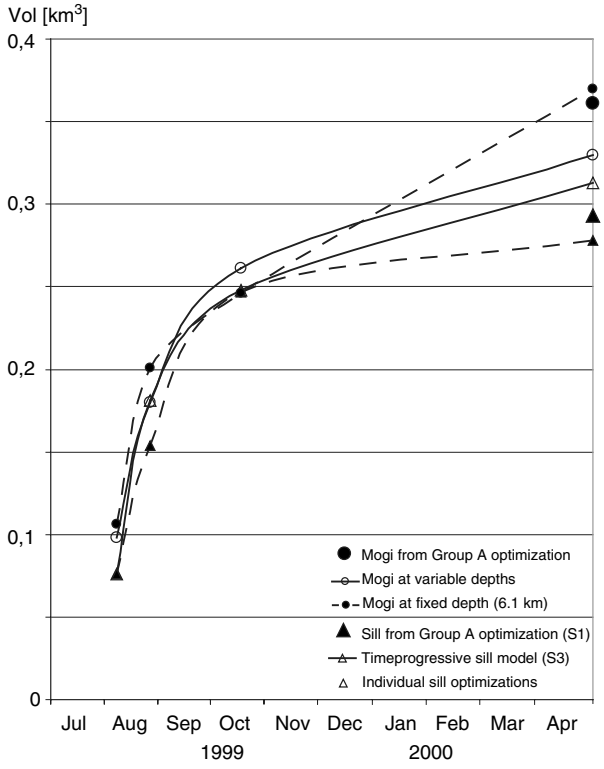

Fig. 12 Accumulated magma volume vs. time. May 1, 2000 is chosen as the ending time for the intrusion, as GPS indicates that the deformation ceased between February and early May, 2000 (Sturkell et al. 2003)

(Fig. 2d), whereas no crustal deformation was detected in the Eyjafjallajökull area before mid-July.

Magmatic flow-rate

For both the point and plane source modeling results, we obtained a rough estimate of the variation in magmatic flux rates throughout the 1999 Eyjafjallajökull intrusion. The inferred accumulated magma volumes are plotted against time in Fig. 12. The flow rate is highest in the initial phase of the intrusion, and declines after a few weeks. A similar pattern has been observed during diking events in northern Iceland, though at a different timescale (Tryggvason 1980). Declining flow rates are also found in studies of re-inflating magma chambers (e.g., Björnsson et al. 1979; Lu et al. 2003) and is furthermore a characteristic of volcanic eruptions (e.g., Gudmundsson et al. 1992; Gudmundsson et al. 2004). The decline in flow rate may be caused by a reduction in overpressure within the magmatic system. By extrapolation of the volume curves to intersect the time axis (Fig. 12), a rough estimate of the onset time of the intrusion is obtained and is deduced to be in the second half of July. Deformation associated with the earthquake swarm activity has previously been interpreted as having started after July 19 based on surface tilt measurements (Sturkell et al. 2003).

If we assume that the volumetric expansion due to the intrusion in Eyjafjallajökull started around mid-July, as indicated by Fig. 12, we can calculate the average magmatic flow rate for the initial phase of the intrusion. Until August 25, a total of 0.015–0.020 km^3 magma were intruded into the system, giving a magmatic flux rate (Q) of 4–6 m^3/s, comparable to the average rate of 5 m^3/s observed for inflow of magma towards shallow levels during the initial part of the Krafla rifting episode in northern Iceland (e.g., Björnsson et al. 1979). For simplicity, we consider magma movements to be driven by buoyancy forces with sill formation occurring at the level of neutral buoyancy. If we assume that the inflowing magma is transported by laminar flow in a single cylindrical pipe, we can estimate the required radius of this pipe, through the relation

$$Q = (\pi/8) \times \Delta\rho \times g \times R^4 \times \mu^{-1}, \quad (3)$$

where $\Delta\rho$ is the density difference between melt and surrounding rock, g is the gravitational constant, R is the pipe radius and μ is the viscosity of the melt (Turcotte and Schubert 2002). As R is in the fourth power, the pipe radius estimate is relatively robust for a range of $\Delta\rho$ and μ. For basaltic melts magma viscosity, μ, ranges between 10–100 Pa/s (Spera 2000), melt density was set to 2,650 kg/m^3 (Spera 2000) and with host rock density at 2,950—3,135 km/m^3 (Turcotte and Schubert 2002; Gudmundsson 2003), we obtain $R<1$ m. The high value for host rock density corresponds to dense lower crust (Gudmundsson 2003). A pipe with a diameter of 1–2 m at 6 km depth would not be expected to produce any significant surface deformation, but may have a localized effect on the stress state of the surrounding rocks and trigger micro-earthquake activity, in particular during the initial opening phase.

Internal volcano growth

The intrusive events in 1994 and 1999 caused an extensive surface area of the Eyjafjallajökull volcano to uplift, thereby amplifying the topography of the volcano. Within Iceland, significant topographic relief is to a large degree found outside the main rift zones, despite the fact that the rift zones are the sites of the highest volcanic production. However, the high heat production and young crust in the rift zones causes low flexural rigidity, facilitating rapid subsidence in response to the loading by volcanic products as described by Pálmason (1973). Furthermore, the tensional setting facilitates destruction of volcanic edifices, and high topographic relief is therefore largely restricted to volcanic flank zones.

Eyjafjallajökull is situated within the volcanic flank zone, south of the junction between the EVZ and the SISZ. Intrusion of sills may be an important mechanism contributing to the internal growth of it as well as other volcanoes. If we assume that similar events as the combined effect of the 1994 and 1999 intrusions happen within Eyjafjallajökull on average once every few hundred years, we obtain an inter-

nal growth rate of ~15 cm/century. Since the volcano is as old as >0.78 Ma (Kristjansson et al. 1988), Eyjafjallajökull may have grown internally by up to 1 km. We do not imply that this is a steady-state process, but merely indicate that the setting of a volcano within a flank zone may favor intrusion of sills, as significant topographic relief, being distinct from the extensional environment reigning in the rift-zones, combined with low spreading rates perturbs the local stress regime. Sill intrusions facilitate internal growth and could in fact contribute significantly to the creation of the characteristic high topography within the Icelandic flank zones. Internal growth by sill intrusion may be an important process at other volcanoes as well. For example, a study by Staudigel and Schmincke (1984) of a 6 km thick continuously exposed volcanic/plutonic series of La Palma, Canary Islands, shows that the basement complex is comprised of more than 50% of intrusive rocks mainly in the form of sills and each being less than a meter thick.

Comparison to other studies:

The modeled deformation source at Eyjafjallajökull deviates geometrically from what has previously been found for volcanoes in Iceland. Mogi point sources have successfully been applied to deformation data from Askja (Tryggvason 1989; Sturkell and Sigmundsson 2000), Hekla (Tryggvason 1994), and Hengill (Sigmundsson et al. 1997b; Feigl et al. 2000) and a combination of point source(s) and dilatational dike geometry at Krafla (e.g., Árnadóttir et al. 1998; Sigmundsson et al. 1997a; de Zeeuw-van Dalfsen et al. 2004) and Hekla (Linde et al. 1993). These volcanic systems are, however, all situated at extensional rifting segments, making up the active plate boundary in Iceland (Fig. 1) and, hence, either favor dike intrusion due to the dilatational background stresses or have established magma chambers at crustal levels. Askja and Krafla are examples of volcanoes with established magma chambers, and are expected to exhibit deformation patterns reproducible by pressurization or depressurization of spherical source geometries. However, the location of Eyjafjallajökull volcano within a volcanic flank zone, where extension is minor compared to the active spreading zones, may provide a locally perturbed stress field at depth. Compressive stresses, created by the load of the considerable volcanic structure, may even dominate. A local compressive stress field in combination with the lack of a residing magma chamber at crustal levels favors sills as the preferred geometry of shallow intrusions within this system.

The level of seismic activity associated with the intrusive events at Eyjafjallajökull has been relatively low compared to previously studied cases of magma migration within the Icelandic crust. In the past, Iceland has been the site of several outstanding examples of earthquake swarms related to magmatic activity. One example is the Krafla rift zone in North Iceland, which experienced numerous earthquake swarms associated with magmatic movements during the most recent rifting episode (1975–1984). Deflations of Krafla volcano were accompanied by rapid migration of earthquake activity both southward along the plate boundary (Brandsdóttir and Einarsson 1979) and northward (Einarsson and Brandsdóttir 1980). The earthquake swarms were clearly coupled to dike injections, and gravity and leveling measurements confirm magma transport from a shallow magma chamber at Krafla (Björnsson et al. 1979). Strong extensional background stresses may have favored rapid magma movements at very shallow depths, in turn triggering high seismicity levels during the relatively short events (a few days) as opposed to the long lasting, deep intrusive events reported at Eyjafjallajökull volcano. Hence, the magmatic flow rate as well as the depth of intrusion appears to be critical factors controlling the intensity of a seismic crisis arising from subsurface magma movements, whereas the magma volume may not be as important.

Another example where magma transport at crustal levels triggered elevated earthquake activity, is the unusually persistent swarm activity in the Hengill triple junction during 1994–1999 (Sigmundsson et al. 1997b; Feigl et al. 2000; Clifton et al. 2002). During the 5-year period roughly 80,000 events were recorded, most with $M_L<4$. The earthquake swarm coincided temporally with a 2-cm/year surface-uplift rate, interpreted as being caused by an expanding Mogi point source at a depth of about 7 km. It was suggested that the expanding Mogi source increased the level of shear stress, triggering extensive earthquake activity (Sigmundsson et al. 1997b), including episodic slip on faults as seen in the $M_L5.0$ and $M_L5.1$ events in 1998 Feigl et al. 2000). The magmatic intrusions at Hengill and Eyjafjallajökull are modeled at comparable depths, hence their difference in associated seismicity must arise from some other controlling factor. The Hengill system is situated within an active spreading segment of the plate boundary where background stresses are high. An increase in stressing rate will, therefore, trigger a higher level of earthquake activity since the crust within the spreading zones may be closer to failure than in the more stable tectonic setting of the Eyjafjallajökull volcano.

Subsurface magma movements causing what appears to be a minor seismic crisis situated in a tectonically relatively stable environment, may be equivalent to those associated with a major seismic crisis in more dynamic tectonic settings. This is because the level of seismic activity has to be viewed in the light of at least the following controlling factors: magmatic flow rate, depth of intrusion and in particular the reigning background stresses.

Conclusions

A total of ~0.03 km^3 magma entered the Eyjafjallajökull volcanic system during an intrusive episode in 1999. A study of surface deformation evaluated together with a pattern analysis of earthquake locations enables spatio-temporal visualization of magma migration at depth during sill formation, and localization of the site of a possible narrow feeder channel in the northern flank of the

volcano. The magmatic flow rate was initially estimated at about 4–6 m^3/s, decreasing through time. The study was facilitated by the excellent spatial and fortunate temporal coverage of the InSAR images used.

Because magma chamber inflation would result in a fairly constant model source location through the duration of the intrusion, the Eyjafjallajökull volcano is interpreted as being a cold structure without a magma chamber at a shallow depth. In consideration of the magmatic overpressure required, a cold structure will favor sheet-like intrusions rather than spherical sources. A sill model at a depth of 6.3 km, experiencing variable amounts of opening through time, explains the InSAR data well. GPS measurements and predictions calculated from our InSAR based modeling results are in reasonable agreement, and earthquake locations support a sill model. Sill intrusions may be an important internal growth process occurring in the Icelandic flank zone volcanoes, thereby contributing to their considerable topographic relief.

Acknowledgements We thank Editor Hiroshi Shinohara, reviewer Akira Takada as well as an anonymous reviewer for suggestions which helped to improve the paper. Alan Linde, Tim Wright, Páll Einarsson and Thóra Árnadóttir are thanked for valuable comments on an earlier version of the manuscript. We thank Bryndís Brandsdóttir for scientific discussions and access to unpublished earthquake locations. Kristín Vogfjörd and Erik Sturkell from the Icelandic Meterological Office are thanked for supplying data from the SIL network and GPS data, respectively. ERS SAR images were provided through ESA Envisat grant A03-22 and ERS grant A03-200. Personal grants to RP from the Icelandic science foundation (Rannís, Grants 020110002 and 040202041) and to FS from the University of Iceland Research Fund are acknowledged, as well as support from the EU-supported RETINA project (grant EVG1-CT-0044) and PREPARED project (grant EVG1-CT-2002-00073). The GMT public domain software was used to prepare Fig. 1.

References

Amelung F, Jónsson S, Zebker H, Segall P (2000) Widespread uplift and "trapdoor" faulting on Galápagos volcanoes observed with radar interferometry. Nature 407:2–996

Árnadóttir T, Sigmundsson F, Delaney PT (1998) Sources of crustal deformation associated with the Krafla, Iceland, eruption of September 1984. Geophys Res Lett 25:2–1046

Björnsson A, Johnsen G, Sigurdsson S, Thorbergsson G, Tryggvason E (1979) Rifting of the plate boundary in North Iceland 1975–1978. J Geophys Res 84:2–3038

Brandsdóttir B, Einarsson P (1979) Seismic activity associated with the September 1977 deflation of the Krafla volcano in northeastern Iceland. J Volcanol Geotherm Res 6:2–212

Brandsdóttir B (2000) Earthquakes and magma under Mýrdalsjökull and Eyjafjallajökull (in Icelandic). In: Abstracts of the Geoscience Society of Iceland Spring 2000 Meeting, Reykjavik 3–4

Bövarsson R, Rögnvaldsson ST, Slunga R, Kjartansson E (1999) The SIL data acquisition system: at present and beyond year 2000. Phys Earth Planet Int 113:2–101

Cervelli P, Murray MH, Segall P, Aoki Y, Kato T (2001) Estimating source parameters from deformation data, with an application to the March 1997 earthquake swarm off the Izu Peninsula, Japan. J Geophys Res 106:2–11237

Clifton AE, Sigmundsson F, Feigl KL, Gumundsson G, Árnadóttir T (2002) Surface effects of faulting and deformation resulting from magma accumulation at the Hengill triple junction, SW Iceland, 1994-1998. J Volcanol Geotherm Res 115:2–255

C.N.E.S (1997) DIAPASON/PRISME Software, Toulouse, France

Dahm T, Brandsdóttir B (1997) Moment tensors of microearthquakes from the Eyjafjallajökull volcano in South Iceland. Geophys J Int 130:2–192

de Zeeuw-van Dalfsen E, Pedersen R, Sigmundsson F, Pagli C (2004) Deep accumulation of magma near the crust-mantle boundary at the Krafla volcanic system, Iceland: Evidence from Satellite Radar Interferometry 1993–1999. Geophys Res Lett 31:L13611, doi:10.1029/2004GL020059

Dvorak JJ, Dzurisin D (1997) Volcano geodesy: the search for magma reservoirs and the formation of eruptive vents. Rev Geophys 35:2–384

Dzurisin D (2003) A comprehensive approach to monitoring volcano deformation as a window on the eruption cycle. Rev Geophys 41:2, doi:1010.1029/2001RG000107

Einarsson P, Brandsdóttir B (1980) Seismological evidence for lateral magma intrusion during the July 1978 deflation of the Krafla volcano in NE-Iceland. J Geophys 47:2–165

Einarsson P, Sæmundsson K (1987) Earthquake epicenters 1982-1985 and volcanic systems in Iceland. In: Sigfússon T (ed) Í Hlutarsins Eli, Festschrift for Thorbjorn Sigurgeirsson. Menningarsjóur, Reykjavík (map)

Einarsson P, Brandsdóttir B (2000) Earthquakes in the Mýrdalsjökull area, Iceland, 1978–1985: seasonal correlation and connection with volcanoes. Jökull 49:2–73

Feigl KL, Gasperi J, Sigmundsson F, Rigo A (2000) Crustal deformation near Hengill volcano, Iceland 1993–1998: coupling between magmatic activity and faulting inferred from elastic modeling of satellite radar interferograms. J Geophys Res 105:25,655–25,670

Gudmundsson A, Oskarsson N, Gronvold K, Saemundsson K, Sigurdsson O, Stefansson R, Gislason SR, Einarsson P, Brandsdottir B, Larsen G, Johannesson H, Thordarson T (1992) The 1991 eruption of Hekla, Iceland. Bull Volcanol 54:2–246

Gudmundsson Ó (2003) The dense root of the Iceland crust. Earth Planet Sci Lett 206:2–440

Gudmundsson MT, Sigmundsson F, Björnsson H, Högnadóttir T (2004) The 1996 eruption at Gjálp, Vatnajökull ice cap, Iceland: efficiency of heat transfer, ice deformation and subglacial water pressure. Bull Volcanol 66:2–65

Gudmundsson MT, Elíasson J, Larsen G, Gylfason ÁG, Einarsson P, Jóhannesson T, Hákonardóttir KM, Torfason H (2005) Overview on the dangers of volcanic eruptions and floods from the western part of Mýrdalsjökull and Eyjafjallajökull (in Icelandic), In: Gudmundsson MT, Gylfason ÁG (eds) Hættumat vegan eldgosa og hlaupa frá vestanverdum Mýrdalsjökli og Eyjafjallajökli, Ríkislögreglustjórninn, Háskólaútgáfan, 11–44

Gudmundsson S, Carstensen JM, Sigmundsson F (2002) Unwrapping ground displacement signals in satellite radar interferograms with the aid of GPS data and MRF regularization. IEEE Trans Remote Sensing Geosci 40:2–1754

Haimson BC, Rummel F (1982) Hydrofracturing stress measurements in the Iceland research drilling project drill hole at Reydarfjordur, Iceland, J Geophys Res 87:2–6649

Jakobsdóttir SS, Gumundsson GB, Stefánsson R (2002) Seismicity in Iceland 1991–2000 monitored by the SIL seismic system. Jökull 51:2–94

Jónsson S, Zebker H, Cervelli P, Segall P, Garbeil H, Mouginis-Mark P, Rowland S (1999) A shallow-dipping dike fed the 1995 flank eruption at Fernandina volcano, Galápagos, observed by satellite radar interferometry. Geophys Res Lett 26:2–1080

Jónsson S, Zebker H, Segall P, Amelung F (2002) Fault slip distribution of the 1999 Mw7.1 Hector Mine, California, earthquake, estimated from satellite radar and GPS measurements. Bull Seismol Soc Am 92:2–1389

Kristjánsson L, Jóhannesson H, Eiríksson J, Gudmundsson AI (1988) Brunhes: Matuyama paleomagnetism in three lava sections in Iceland. Can J Earth Sci 25:2–225

Linde AT, Águstsson K, Sacks IS, Stefansson R (1993) Mechanism of the 1991 eruption of Hekla from continuous borehole strain monitoring. Nature 365:2–740

Lister JR, Kerr RC (1991) Fluid-mechanical models of crack propagation and their application to magma transport in dykes. J Geophys Res 96:2–10077

Lu Z, Masterlark T, Dzurisin D, Rykhus R, Wicks Jr. C (2003) Magma supply dynamics at Westdahl volcano, Alaska, modeled from satellite radar interferometry. J Geophys Res 108:2, doi:2310.1029/2002JB002311

Massonnet D, Feigl KL (1998) Radar interferometry and its application to changes in the Earth's surface. Rev Geophys 36:2–500

Massonnet D, Sigmundsson F (2000) remote sensing of volcano deformation by radar interferometry from various satellites. In: Mouginis-Mark PJ, Crisp JA, Fink JH (eds) Remote Sensing of Active Volcanism 116. AGU, Washington DC, 207–221

Mogi K (1958) Relations between the eruptions of various volcanoes and the deformation of the ground surfaces around them. Bull Earthqua Res Inst 36:2–134

Okada Y (1985) Surface deformation due to shear and tensile faults in a half-space. Bull Seismol Soc Am 75:2–1154

Okada Y, Yamamoto E (1991) Dyke intrusion model for the 1989 seismovolcanic activity off Ito, central Japan. J Geophys Res 96:2–10376

Pálmason G (1973) Kinematics and heat flow in a volcanic rift zone, with application to Iceland. Geophys J Royal Astronom Soc 33:2–481

Pedersen R, Jónsson S, Árnadóttir T, Sigmundsson F, Feigl KL (2003) Fault-slip distribution of two June 2000 Mw6.5 earthquakes in South Iceland estimated from joint inversion of InSAR and GPS measurements. Earth Planet Sci Lett 213:2–502

Pedersen R, Sigmundsson F (2004) InSAR based sill model links spatially offset areas of deformation and seismicity for the 1994 unrest episode at Eyjafjallajökull volcano, Iceland. Geophys Res Lett 31:L14610, doi:10.1029/2004GL020368

Pritchard ME, Simons M (2002) A satellite geodetic survey of large-scale deformation of volcanic centres in the central Andes. Nature 418:2–171

Sigmundsson F (1996) Crustal deformation at volcanoesIn: Barberi F, R Casale (eds) Proceedings of the course: The Mitigation of Volcanic Hazards, European School of Climatology and Natural Hazards, 12–18 June 1994, Vulcano, Sicily, 237–257.

Sigmundsson F, Vadon H, Massonnet D (1997a) Readjustment of the Krafla spreading segment to crustal riftingmeasured by satellite radar interferometry. Geophys Res Lett 24:2–1846

Sigmundsson F, Einarsson P, Rögnvaldsson ST, Foulger GR, Hodgkinson KM, Thorbergsson G (1997b) The 1994–1995 seismicity and deformation at the Hengill triple junction, Iceland: triggering of earthquakes by minor magma injection in a zone of horizontal shear stress. J Geophys Res 102:15151–15161

SIL database (2004) Icelandic Meteorological Office. http://hraun.vedur.is/cgi-bin/sellib

Spera FJ (2000) Physical properties of magmas. In: Sigurdsson H (ed) Encyclopedia of volcanoes. Academic Press, New York, 171–190

Staudigel H, Schmincke H-U (1984) The Pliocene seamount series of La Palma/Canary Islands. J Geophys Res 89:2–11215

Stefánsson R, Bövarsson R, Slunga R, Einarsson P, Jakobsdóttir S, Bungum H, Gregersen S, Havskov J, Hjelme J, Korhonen H (1993) Earthquake prediction research in the south Iceland seismic zone and the SIL project. Bull Seismol Soc Am 83:2–716

Sturkell E, Sigmundsson F (2000) Continuous deflation of the Askja caldera, Iceland, during the 1983–1998 noneruptive period. J Geophys Res 105:2–25684

Sturkell E, Sigmundsson F, Einarsson P (2003) Recent unrest and magma movements at Eyjafjallajökull and Katla volcanoes, Iceland. J Geophys Res 108:2, doi:2310.1029/2001JB000917

Sæmundsson K (1979) Outline of the geology of Iceland. Jökull 29:2–28

Toda S, Stein RS, Sagiya T (2002) Evidence from the AD 2000 Izu islands earthquake swarm that stressing rate governs seismicity. Nature 419:2–61

Tryggvason E (1980) Subsidence events in the Krafla Area, North Iceland, 1975-1979. J Geophys 47:2–153

Tryggvason E (1989) Ground deformation in Askja, Iceland: its source and possible relation to flow of the mantle plume. J Volcanol Geotherm Res 39:2–71

Tryggvason E (1994) Observed ground deformation at Hekla, Iceland prior to and during the eruptions of 1970, 1980–1981 and 1991. J Volcanol Geotherm Res 61:2–291

Turcotte DL, Schubert G (2002) Geodynamics (2.nd edn), Cambridge University Press, Cambridge

Welstead ST (1999) Fractal and wavelet image compression techniques. SPIE Optical Engineering Press, Bellingham, WA p 232.